JOURNAL OF GEOPHYSICAL RESEARCH, VOL. 115, D03303, doi:10.1029/2009JD012734, 2010

Subgrid-scale treatment for major point sources in an Eulerian model: A sensitivity study on the European Tracer Experiment (ETEX) and Chernobyl cases

Irène Korsakissok[1] and Vivien Mallet[2]

Received 25 June 2009; revised 28 August 2009; accepted 28 September 2009; published 11 February 2010.

[1] We investigate the plume-in-grid method for a subgrid-scale treatment of major point sources in the passive case. This method consists in an online coupling of a Gaussian puff model and an Eulerian model, which better represents the point emissions without significantly increasing the computational burden. In this paper, the plume-in-grid model implemented on the Polyphemus air quality modeling system is described, with an emphasis on the parameterizations available for the Gaussian dispersion, and on the coupling with the Eulerian model. The study evaluates the model for passive tracers at continental scale with the European Tracer Experiment (ETEX) and the Chernobyl case. The aim is to (1) estimate the model sensitivity to the local-scale parameterizations and (2) bring insights on the spatial and temporal scales that are relevant in the use of a plume-in-grid model. It is found that the plume-in-grid treatment improves the vertical diffusion at local scale, thus reducing the bias, especially at the closest stations. Doury's Gaussian parameterization and a column injection method give the best results. There is a strong sensitivity of the results to the injection time and the grid resolution. The "best" injection time actually depends on the resolution but is difficult to determine a priori. The plume-in-grid method is also found to improve the results at fine resolutions more than with coarse grids by compensating the Eulerian tendency to overpredict the concentrations at these resolutions.

Citation: Korsakissok, I., and V. Mallet (2010), Subgrid-scale treatment for major point sources in an Eulerian model: A sensitivity study on the European Tracer Experiment (ETEX) and Chernobyl cases, *J. Geophys. Res.*, *115*, D03303, doi:10.1029/2009JD012734.

1. Introduction

1.1. Context

[2] Classical air quality models at regional scale, based on Eulerian approaches, overlook subgrid-scale phenomena. In particular, emissions from major point sources are badly represented by Eulerian models since they are usually assumed to mix immediately within a grid cell, whereas a typical point-source plume (e.g., from a power plant) does not expand to the size of the grid cell for a substantial time period. This leads to an unrealistic near-source modeling, especially since the K-theory approach often used in Eulerian models does not properly represent the diffusion in the vicinity of the source [*Maryon and Buckland*, 1995]. Numerical problems can also be raised, such as oscillations caused by strong gradients due to point sources [*Brandt et al.*, 1996], if a nonmonotonic advection scheme is used. On the other hand, Gaussian models provide a better representation of the near-source dispersion, but they rely on assumptions (e.g., no wind shear) that lead to increasing errors on the plume trajectory with distance [*Stohl*, 1998].

[3] The plume-in-grid method is a multiscale modeling technique that couples a Gaussian (plume or puff) model with an Eulerian model in order to improve the treatment of point source emissions. This coupling method has been developed and evaluated both for photochemical applications [e.g., *Seigneur et al.*, 1983; *Morris et al.*, 1991; *Kumar and Russell*, 1996; *Byun and Schere*, 2006; *Karamchandani et al.*, 2002] and for the modeling of accidental releases with the DREAM model [*Brandt*, 1998].

1.2. Issues

[4] This paper is aimed at investigating some issues of this multiscale modeling approach.

1.2.1. Physical Processes

[5] The theoretical reasons why such a coupling would improve the near-source dispersion are well known, but we seek to have an insight on the key physical processes (e.g., horizontal or vertical diffusion) for which a subgrid-scale treatment is most relevant. One may also wonder whether the largest impact would show on the plume travel time, or on the concentrations.

1.2.2. Local-Scale Parameterizations

[6] Another question is the sensitivity of both the local-scale and the large-scale models to the input parameters and the dispersion schemes. This issue was already addressed by

[1]CEREA, Université Paris Est, Champs-sur-Marne, France.
[2]INRIA, Paris-Rocquencourt Research Center, Le Chesnay, France.

0148-0227/10/2009JD012734$09.00

Brandt et al. [1998] with a focus on the sensitivity to the Eulerian parameterizations, and by *Brandt* [1998] where results with several Gaussian parameterizations were also briefly compared. Here, the sensitivity to the Gaussian dispersion is highlighted, and compared to the impact of the Eulerian vertical diffusion schemes.

1.2.3. Relevant Time and Spatial Scales

[7] It is also crucial to estimate the relevant spatial and time scales for both models. The "local scale" is the scale at which the use of a Gaussian model is relevant. It is the near-source area where the dispersion is not well represented by the Eulerian model, and the Gaussian model error due to trajectory uncertainties and wind shear is not too large. When the improvements in the dispersion are outweighed by the uncertainties in the plume trajectory, the plume must be transferred from the Gaussian model to the Eulerian model. This injection is decided according to some criterion on the puff age or size. For instance, in several photochemical plume-in-grid models, the transfer is done when the puff size is about the Eulerian grid size at the transfer time. In DREAM, the Gaussian model is used on a nested subdomain, whose size is determined so that the puffs would be larger than the Eulerian cell size at the interface, where the puffs are transferred into the Eulerian model. These conditions are physically consistent with the primary goal of plume-in-grid models, that is, to minimize the artificial horizontal dilution. However, this does not prevent large errors in the plume trajectory in the case of very coarse grids. Alternatively, some models use a criterion on the plume travel time, usually 1 h (e.g., in work by *Kumar and Russell* [1996]), but no sensitivity study is available on the subject. This issue is investigated here by means of a sensitivity study on the so-called "injection time" for a wide range of values. A comparison is also made between the time and size criteria, at several resolutions.

1.2.4. Relevant Resolution

[8] Finally, we investigate whether the use of the plume-in-grid modeling technique is more relevant at a low or high resolution. In theory, a low resolution would imply more artificial dilution in the Eulerian model, hence more need for a subgrid-scale representation of the plume. In practice, using fine resolutions do not always improve simulation results, especially when no high-resolution input data is used. Thus, it is useful to have an insight on that subject, and to issue, if possible, general recommendations about the resolutions and corresponding injection times.

1.3. Methodology

[9] These issues are investigated using the plume-in-grid model developed on the air quality modeling system Polyphemus [*Mallet et al.*, 2007]. This model was developed both for photochemistry and passive (chemically inert) tracers, at regional and continental scale. The aim is to provide an easy-to-use and modular model that is appropriate for a wide range of applications and modeling domains, with limited computational demands. The model can be used in the context of operational applications where detailed meteorological fields are not always available, and computational time constraints do not allow high-resolution or adaptive grid simulations.

[10] The model evaluation is carried out for passive-tracer releases with ETEX-1 (European Tracer Experiment, first release) and Chernobyl cases. The ETEX campaign provides an appropriate case to carry out a detailed study, since it is well documented and the source parameters are well known, thus reducing the uncertainties. The plume-in-grid model, with the recommendations inferred from the ETEX sensitivity study, is then evaluated on the Chernobyl case.

1.4. Outline

[11] Section 2 describes the model, with an emphasis on the local-scale model and the coupling methods. In sections 3, 4, 5 and 6, the aforementioned issues (section 1.2) are investigated on the ETEX case: section 3 analyzes the results with/without plume-in-grid, section 4 discusses the sensitivity to the local-scale dispersion parameters, compared to the Eulerian diffusion schemes, section 5 details the model sensitivity to the puff injection time and section 6 gives an insight on the influence of the grid resolution. Finally, section 7 gives the overall model results on the Chernobyl case.

2. Model Description

[12] The plume-in-grid model presented here couples, on the Polyphemus platform, the Gaussian puff model [*Korsakissok and Mallet*, 2009] with the Eulerian model Polair3D [*Boutahar et al.*, 2004]. In section 2.1, we briefly present the Gaussian puff model, and the necessary adjustments made to the Gaussian dispersion for the nonstationary case. Section 2.2 describes the method used to couple the two models.

2.1. Gaussian Puff Model

2.1.1. Model Presentation

[13] The Gaussian puff model represents a continuous point emission as a series of Gaussian puffs. Each puff transports a given quantity of the emitted species; the speed and the direction of a puff are determined by the wind at its center. The puff size increases with turbulence, and it is determined by the Gaussian standard deviations in all three directions: σ_x (downwind), σ_y (crosswind) and σ_z (vertical). The concentration at one point (x, y, z) is then given by the sum of all the puffs' contributions,

$$C(x,y,z) = \sum_{i=1}^{N_{\text{puff}}} \frac{Q_s \times \Delta t_{\text{puff}}}{(2\pi)^{3/2}\sigma_x\sigma_y\sigma_z} \exp\left(-\frac{\left(x-x_c^i\right)^2}{2\sigma_x^2}\right) \times \exp\left(-\frac{\left(y-y_c^i\right)^2}{2\sigma_y^2}\right) \exp\left(-\frac{\left(z-z_c^i\right)^2}{2\sigma_z^2}\right), \quad (1)$$

where N_{puff} is the number of puffs, Δt_{puff} is the time step between the release of two consecutive puffs, and (x_c^i, y_c^i, z_c^i) are the coordinates of the center of the ith puff. Q_s is the source emission rate (in mass unit per second). Equation (1) can be modified to take into account the reflections on the ground and elevated inversion layer if necessary. The continuous plume is well represented by the series of puffs if there is a sufficient overlap between two successively released puffs, that is, if Δt_{puff} is small enough. In practice, this condition is fulfilled at time t, for two successive puffs emitted at t_i and $t_{i+1} = t_i + \Delta t_{\text{puff}}$, if

$$\sigma_x(t-t_i) + \sigma_x(t-t_{i+1}) \geq u\Delta t_{\text{puff}}, \quad (2)$$

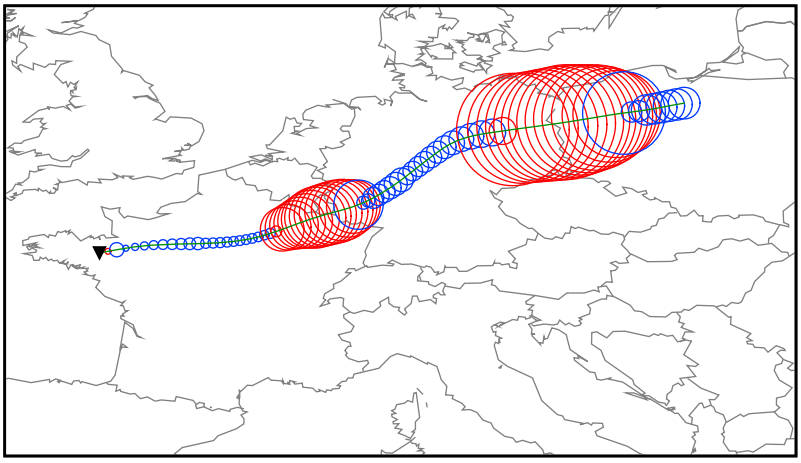

Figure 1. Unrealistic evolution of the size of one puff without correction on σ_y. The puff is represented at each time step, and the circle radius is proportional to σ_y. The puffs are drawn in red when it is daytime and in blue during nighttime. The green line is the puff center. The black triangle is the source location.

where u is the wind speed at time t and at the puffs' locations, and the puffs' sizes ("radii") are assumed to be $\sigma_x(t - t_i)$ and $\sigma_x(t - t_{i+1})$ in the x direction. This criterion can be relaxed during the first time steps, when no measurement station has been reached: the overlap condition has to be fulfilled at the first station. Section 3.2 discusses this condition in the present case.

[14] In Polyphemus, three empirical parameterizations may be used to compute puffs standard deviations: Briggs's, Doury's and similarity theory. They are briefly described below, and more details are given by *Korsakissok and Mallet* [2009], along with a validation against the Prairie Grass and Kincaid data sets.

2.1.1.1. Briggs's Formulae

[15] The Briggs formulae are based on the Pasquill-Turner stability classes [*Turner*, 1969], and are different for rural and urban areas. The full formulae are given by *Arya* [1999] for instance. The general form is given by

$$\sigma_y = \frac{\alpha x}{\sqrt{1+\beta x}}, \qquad \sigma_z = \alpha x (1+\beta x)^{\gamma}, \tag{3}$$

with x the downwind distance from source, and α, β and γ coefficients depending on Pasquill stability class.

2.1.1.2. Doury's Formulae

[16] An alternative parameterization, developed for the specific application of radionuclides dispersion, is described by *Doury* [1976]. The formulae use only two stability situations, corresponding to normal and low dispersion. The standard deviations are given in the general form

$$\sigma_y = (A_h t)^{K_h}, \qquad \sigma_z = (A_z t)^{K_z}, \tag{4}$$

where t is the puff "age" (time since the puff release), and A_h, A_z, K_h and K_z are coefficients depending on the stability and the puff time.

2.1.2. Similarity Theory

[17] If enough meteorological data is available, σ_y and σ_z can be estimated using the standard deviations of wind velocity fluctuations in horizontal direction σ_v and in vertical direction σ_w. Following *Irwin* [1979] dispersion coefficients are investigated in the form

$$\sigma_y = \sigma_v t F_y, \qquad \sigma_z = \sigma_w t F_z, \tag{5}$$

where t is the time since the puff release, and F_y and F_z are functions of a set of parameters that characterize the atmospheric boundary layer. These functions are determined from experimental data. Here, the expressions of F_y and F_z, as well as σ_v and σ_w, come from *Irwin* [1979], *Hanna et al.* [1982], *Hanna* [1984] and *Weil* [1988].

2.1.3. Dealing With Nonstationarity: Treatment for Dispersion Parameters

[18] The parameterizations to compute the standard deviations assume that the meteorological situation is stationary and homogeneous, which is not the case in the plume-in-grid model. Hence the need to adapt the usual Gaussian formulations to nonstationary situations. The Gaussian standard deviation in one direction can be written in the general form

$$\sigma = f(t), \tag{6}$$

where t is the puff travel time, and f is a function depending on the meteorological situation. Equation (6) gives the puff evolution assuming that f has been constant since the puff emission time. Using this formula in nonstationary cases, where f is evaluated at each time step with the local meteorological situation, could lead to the unrealistic situation where the puff size would decrease. This would be the case for instance if the situation changed from unstable to stable (e.g., if night has fallen), as illustrated by Figure 1.

[19] A physically consistent way to deal with this problem is to determine the puff growth time step per time step. The local growth of σ is perfectly determined by the value at the beginning of the time step (noted σ_1) and the knowledge of f (equation (6)) for the current situation. Since f is an increasing function of time (for constant meteorological conditions), one may determine the virtual time t'_1 at which the standard deviation value is σ_1: $t'_1 = f^{-1}(\sigma_1)$. The standard deviation at the end of the time step

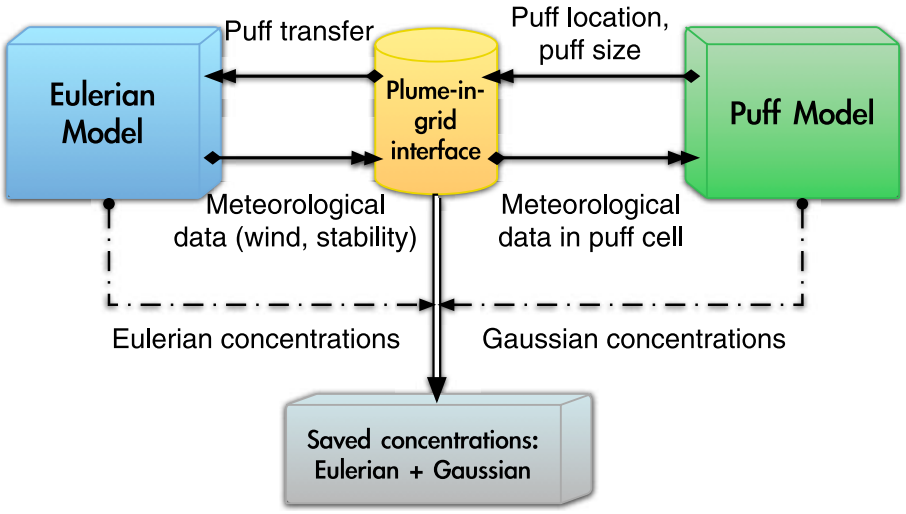

Figure 2. Description of the plume-in-grid coupling: information is exchanged between the Gaussian puff model and the Eulerian model. At each time step the sum of the contributions from both models is saved.

can then be computed as $\sigma_2 = f(t_1' + \Delta t)$. In some cases, however, the inverse function f^{-1} cannot be analytically computed; thus it is only ensured that the puff size cannot decrease during a time step ($\sigma_2 = \max(\sigma_1, f(t_1 + \Delta t))$).

2.2. Model Coupling

[20] In the plume-in-grid coupling, several point source emissions are treated by the Gaussian puff model while other sources, namely diffuse area emissions, are managed by Polair3D. When a puff has reached a given age or size, it is transferred into the Eulerian model. For an emission with a finite duration, the Gaussian puff model is not used anymore after the last puff transfer. During the time period when both models are used, they exchange some information at each time step (Figure 2):

[21] 1. Meteorological data have been computed on the Eulerian grid and can be either interpolated at the puff center or taken at the center of the cell where the puff is located. They are then used by the Gaussian model, to carry out the puff advection and diffusion.

[22] 2. For puff data, at each time step, the cell where the puff center resides is determined. For that purpose, the Cartesian coordinates used in the Gaussian puff model are converted into longitude/latitude coordinates used by Polair3D (Appendix A). It is then checked whether the puff should be injected in the Eulerian model. If so, the puff is erased from the Gaussian puff model, and its mass is transferred into the Eulerian model (section 2.2.1).

2.2.1. Puff Injection Criteria and Method

[23] The puff is transferred to the Eulerian model when one of the two following injection criteria is met:

[24] 1. The time period t_{puff} after the puff release (the puff age) has reached a given value, called the injection time and noted t_{inj}: the injection is applied if $t_{\text{puff}} \geq t_{\text{inj}}$,

[25] 2. The puff horizontal size has reached the cell size Δy: the puff is injected if

$$C_y \sigma_y \geq \Delta y, \tag{7}$$

where C_y is a coefficient usually set to 4.

[26] The puff is then transferred, using either the column, or the integrated injection method.

2.2.1.1. Column Injection

[27] The puff mass is equally distributed within $2\sigma_z$ of the puff center, within one column, bounded by the ground and by the boundary layer height. For a puff within the boundary layer, the puff center height is $z_c \leq z_i$, and the puff vertical extent is given by

$$\min(2\sigma_z, z_c) + \min(2\sigma_z, z_i - z_c). \tag{8}$$

Using the column injection implies that the puff center is "shifted" to the cell center. It also adds some vertical dilution to the extent given in Equation 8: the total vertical extent actually is the sum of the heights of the vertical levels where the transfer is done (Figure 3).

2.2.1.2. Integrated Injection

[28] The puff mass is distributed over the cells within the puff horizontal or vertical extent (Figure 4). In each cell, the puff contribution is the integral of the Gaussian concentration over the cell volume, corrected to ensure the mass conservation (Appendix B). While the column injection limits the artificial puff horizontal dilution, transferring a puff to several cells, as in the integrated-injection method, leads to a higher dilution volume.

2.2.2. Concentrations Reconstructed at the Measurement Stations

[29] Since the two models operate at the same time, the total concentrations are the sum of both models contributions (see Figure 2). Whereas the Eulerian model allows to estimate the mean concentrations in each grid cell, the Gaussian model gives an analytical formula (equation (1)) to compute the concentrations at the exact stations' locations. Therefore, for stations located in the local-scale domain, where the Gaussian model is used, the Gaussian contribution can either be analytically computed at the exact location, or averaged in the grid cells, then interpolated, as with the Eulerian model. Although the first way to reconstruct the concentrations relies on a more accurate repre-

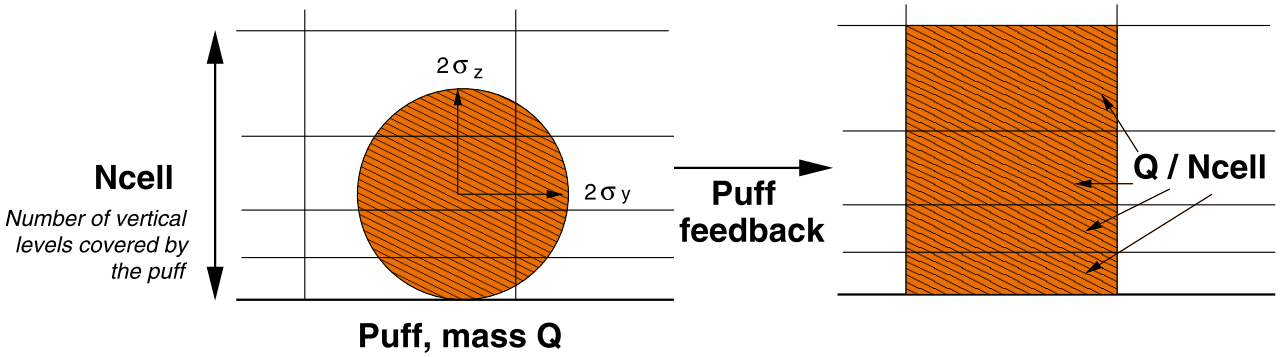

Figure 3. Column injection. The mass Q of the puff is equally distributed in the N_{cell} cells that it vertically covers. The puff vertical extent is $4\sigma_z$ (unless it touched the ground or the inversion layer).

sentation of the Gaussian concentrations, it is more sensitive to the uncertainty in the puff location. If the uncertainty is much larger than the puff horizontal size, the error at the station can be very large. A third option would be to average the concentrations on a volume whose extent would be related to the trajectory uncertainty and would be smaller than a grid cell. The results discussed hereafter are obtained by averaging the concentrations on the grid cells.

3. ETEX Case: Impact of Plume-in-Grid at Continental Scale

[30] The European Tracer Experiment (ETEX) campaign is a well-instrumented, dispersion experiment at continental scale (http://rem.jrc.ec.europa.eu/etex/). We model here the ETEX-I campaign, where 340 kg of a passive tracer (perfluoromethylcyclohexane, hereafter called PMCH) were continuously released during 12 h. The source was located in west of France (48°03′N, 2°00′W; see Figure 1 for the source location). The emission started on 23 October 1994 at 1600 UTC. A total of 168 stations over 17 European countries measured the resulting plume, during more than one week after the release. This experiment was widely used to calibrate and compare atmospheric dispersion models [*Nodop et al.*, 1998; *Mosca et al.*, 1998]. Among the contributions on the subject, several were using Polyphemus with Polair3D: it was evaluated by *Quélo et al.* [2007], and used with inversion methods, for example, by *Bocquet* [2005]. Lagrangian particle models were also evaluated on that case, for instance the NAME model [*Ryall and Maryon*, 1998], as well as Gaussian puff models [*Sorensen*, 1998] and the coupled model DREAM [*Brandt et al.*, 1998].

3.1. Modeling Setup

[31] The configuration is similar to the simulation setup used by *Quélo et al.* [2007]. The simulation grid covers all Europe and its cell width is 0.5625° in longitude and latitude. The source is located at the center of one grid cell. There are 12 vertical levels, up to 6090 m (the first level being at 30 m). The simulation starts at 0000 UTC on 23 October 1994, and the simulation time step is Δt = 600 s. The meteorological fields are the reanalyzed ECMWF fields ERA-40, with resolution 1.125° on the horizontal and with a 3 h time step.

[32] The release height was taken equal to 8 m. The observed plume rise was reported to be no more than 5 m, due to the effect of a significant buoyancy (the ejection temperature is 80°C, the ejection velocity is 47.6 m s^{-1}) moderated by a small source diameter (2.5×10^{-2} m). The plume rise computed by the plume-in-grid model varies during the emission between 1 m and 4 m. In the Eulerian model (alone), the emission is naturally released at the center of the grid cell, whose height is 15 m. The emission rate is 7.98 g s^{-1}.

[33] The plume-in-grid simulations are carried out with the three Gaussian dispersion parameterizations described in section 2.1, and the results are compared with those of

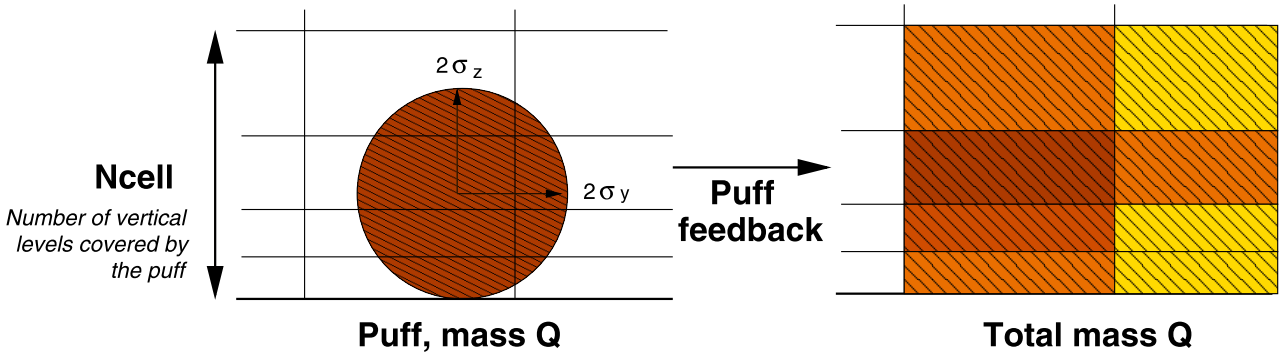

Figure 4. Integrated injection. The puff mass Q is added to each cell within the puff horizontal and vertical extent. The puff vertical extent is $4\sigma_z$ (unless it touches the ground or the inversion layer), and the horizontal size is $4\sigma_y$.

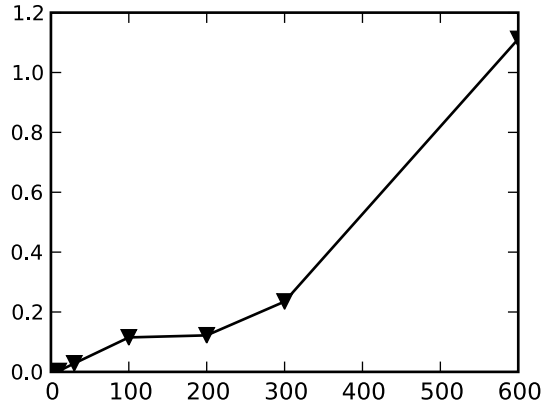

Figure 5. Convergence with the time step between two puffs. The reference is given by the simulation with the time step of 1 s. The indicator is the relative difference between the mean ground concentrations for one time step (between 600 s and 5 s) and the reference value (for 1 s).

Polair3D without the plume-in-grid treatment (hereafter called the "reference" results). Unless specified otherwise, the plume-in-grid results are shown with the column-injection method, which gave slightly better results than the integrated injection.

3.2. Convergence With the Time Step Between Two Puffs

[34] The plume-in-grid model discretizes the emitted plume into a series of puffs. As discussed in section 2.1, the puffs overlap is important to ensure a physically consistent plume modeling. The puff standard deviation after 1 h is about 1000 m (section 4). The mean wind speed is about 5 m s^{-1}. Thus, according to equation (2), a reasonable time step between two puffs is about 400 s, to ensure an overlap at the first station. In comparison, *Sorensen* [1998] used the same condition to compute the puffs overlap, but with different parameterizations for σ_x. They advocated $\Delta t_{\text{puff}} \leq 900$ s.

[35] A sensitivity test was made on the time step between two puffs, to check that the impact of that time step on the simulation results is negligible (for small enough time steps). For that purpose, simulations are carried out with puff time steps of 1, 5, 10, 30, 100, 200, 300 and 600 s. The simulation results are compared with the 1 s simulation, which ensures the best overlap. For all other time steps, the relative difference between the ground concentration and the 1 s simulation ground concentration, averaged in time, is computed in each cell (for concentrations above a threshold of 0.001 ng m^{-3}). The maximum value of this indicator is computed for each time step (Figure 5). Below 200 s, the maximum difference is about 10% of the concentration value, and it is near-zero below 50 s. In the following, the time step between two puffs is taken equal to 5 s in order to ensure a sufficient puffs overlap with a reasonable computational time.

3.3. Comparison of Results With/Without the Plume-in-Grid Approach

[36] The model-to-data comparison is carried out with the following statistical indicators: fractional bias (FB), mean bias error (MBE), correlation (Corr) and proportion of values within a factor 2 and 5 of the observations (FAC2 and FAC5). The formulae are given in Appendix C. These statistics are computed for all stations with a minimum of 11 measurements, which amounts to 139 stations. The measured values are averaged over 3 h. Measurements lower than a threshold of 0.05 ng m^{-3} are discarded, except when they occur within two time intervals (6 h) of a value above the threshold.

3.3.1. Global Results

[37] Table 1 shows the statistics computed for the reference simulation and the plume-in-grid simulation (for the three local-scale configurations) with an injection time equal to 1 h. The use of plume-in-grid improves the results no matter the dispersion parameterization used, reducing the overestimation of the concentrations (from a factor 3 to a factor 2). The correlation is also improved by the use of plume-in-grid with similarity theory and Doury's parameterization, and decreases when using the Briggs formulae. The proportion of values within a factor of 2 and 5 of the observations is slightly improved.

[38] Figure 6 shows how the use of plume-in-grid modifies the spatial distribution of the pollutant concentration. The difference between concentrations with and without plume-in-grid (with similarity theory, 1 h injection time) is computed on ground concentrations, averaged over the whole simulation period. The difference is very high in the vicinity of the source, where the plume-in-grid concentrations are up to 80% lower than the reference concentrations. At farther distance, the concentrations are much lower, and so are the differences. Thus, using the plume-in-grid model mostly modifies the concentrations at a few stations in the vicinity of the source, where the emission is treated by the Gaussian puff model. Reducing the bias at these stations, where the concentrations are the highest, has a significant impact on the overall bias. On the contrary, FAC2 and FAC5 show a smaller improvement, since they are less dependent on the first stations.

3.3.2. Results at Local-Scale Stations

[39] Figure 7 shows a puff's trajectory, and typical size, during 12 h, for Briggs' and similarity theory parameterizations, for a puff emitted at 1600 UTC (Figures 7a and 7b), and a puff emitted a 2200 UTC (Figures 7c and 7d). For all parameterizations, the puffs directly impact one station: Rennes (F21), which is reached between 40 and 60 min after the puff release. The earlier emitted puffs (between 1600 UTC and 2000 UTC), as well as those emitted during the last hour of emission (not shown here) have a straightforward trajectory, and the plume also impacts Alençon

Table 1. Statistics for the Reference Simulation Polair3D, and Plume-in-Grid Simulations With an Injection Time of 60 min for All Three Parameterizations of the Standard Deviations[a]

Model	Mean	FB	MBE	Corr	FAC2	FAC5
Obs	0.21	0.00	0.00	1.00	1.00	1.00
Polair3D	0.68	1.07	0.48	0.60	0.19	0.36
Sim.th.	0.48	0.79	0.27	0.65	0.19	0.37
Doury	0.39	0.61	0.18	0.68	0.20	0.39
Briggs	0.43	0.70	0.22	0.51	0.22	0.39

[a]Column injection. FB, fractional bias; MBE, mean bias error; Corr, correlation; Sim.th., similarity theory.

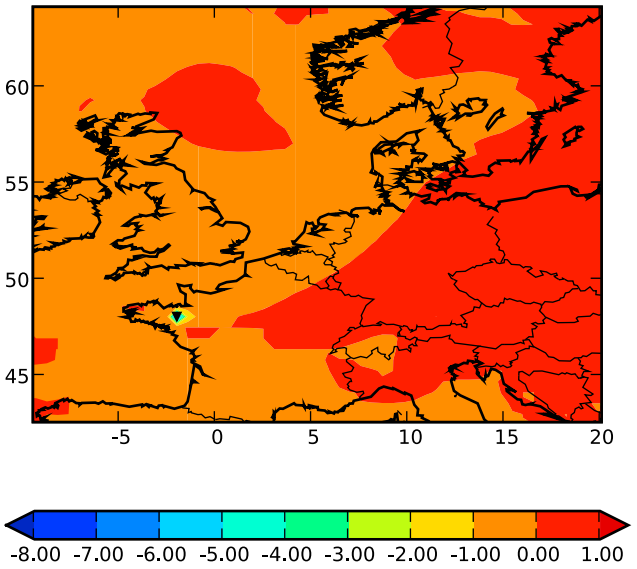

Figure 6. Difference between the mean ground concentrations (in ng m^{-3}) averaged over the simulation period, between the plume-in-grid results and those of the reference simulation. The plume-in-grid simulation was carried out with similarity theory, an injection time of 1 h, and a column injection.

(F02). However, only the station F21 can be considered as a "local-scale" station, reached before the puffs are injected into the Eulerian model.

[40] However the plume-in-grid approach has an impact on a larger scope. We focus now on the "near-source" stations, located within 350 km of the release location, where a high enough number of above-threshold measurements allows to compute significant statistics per station. Most of these stations can be seen in Figure 7 (except station F19 which is southeast from F22, within the main plume trajectory). Table 2 shows the statistics for these stations: the correlation, the MBE, the normalized mean square error (NMSE), the figure of merit in time (FMT), and the FAC5 (see Appendix C). The plume-in-grid results are shown for the Doury parameterization and a 1 h injection time. As expected, the highest impact is found at Rennes, but all other stations show a significant improvement too, especially in terms of NMSE, FMT and FAC5. Thus, the use of plume-in-grid modeling has positive impact at a wider scale than that of the Gaussian model. It is relevant even when few local-scale stations are available: the impact is carried for a few hundreds of kilometers, even though the Gaussian model is used on a much smaller domain. The impact of plume-in-grid at farther stations with lower concentrations is less significant. Essentially no impact is found after about a thousand kilometers.

[41] In section 2.2.2, it was pointed out that the concentrations at local-scale stations (such as Rennes) could also be computed with the analytical Gaussian formula, but this leads to highly overestimated values. As explained, this may come from trajectory errors (due to the wind direction modeling, especially time and space interpolation). If the error in the wind direction is 15% of the traveled distance [*Stohl and Koffi*, 1998], it represents about 3 km when the station is reached, while the puff horizontal "radius" is about 1 km. Moreover, a part of the plume in the upper vertical levels might have been carried away from the main

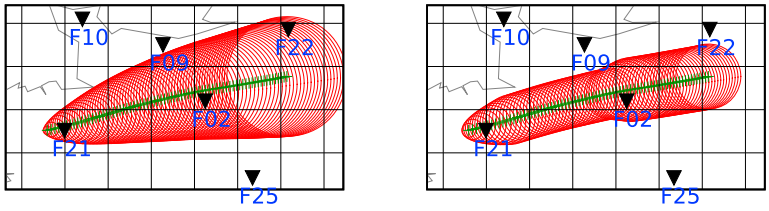

(a) Briggs, Release at 16:00 UTC.

(b) Similarity theory, Release at 16:00 UTC.

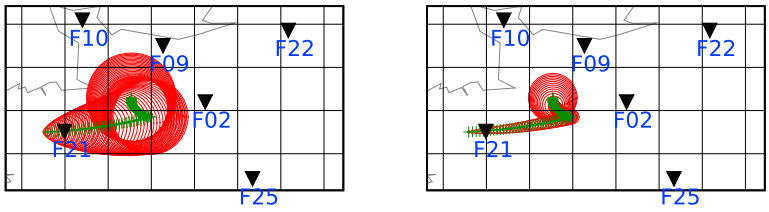

(c) Briggs, Release at 22:00 UTC.

(d) Similarity theory, Release at 22:00 UTC.

Figure 7. Puff trajectory during 12 h. Green is puff center. Red is puff extent represented by a circle with radius 2 × σ_y. One circle is drawn at each time step (10 min). The black triangles are the measurement stations. (a and b) Puff emitted at 1600 UTC. (c and d) Puff emitted at 2200 UTC. Figures 7a and 7c denote Briggs parameterization. Figures 7b and 7d denote similarity theory.

Table 2. Statistics at Stations Located Within 350 km of the Source[a]

Station	MBE	NMSE	Corr	FMT	FAC5
F21	−23.5/−5.0	47.7/8.5	0.69/0.70	0.06/0.22	0/0.18
F02	−3.09/−1.26	12.61/4.25	0.83/0.78	0.16/0.31	0.27/0.33
F22	−1.23/−0.52	13.23/3.97	0.85/0.89	0.15/0.30	0.14/0.21
F19	−1.27/−0.75	5.11/2.34	0.92/0.92	0.29/0.41	0.37/0.50

[a]Statistics are given in this order: reference value/plume-in-grid value. Plume-in-grid values are given for the Doury parameterization and a 60 min injection time. NMSE, normalized mean square error; FMT, figure of merit in time.

trajectory, while the Gaussian model does not account for wind shear.

4. Sensitivity to the Local-Scale Dispersion

[42] Section 3 showed that the near-source concentrations are lower with the plume-in-grid model than with the Eulerian model, especially with the Doury parameterization. This could be surprising, since the use of plume-in-grid is supposed to prevent artificial dilution of the plume. However, this dilution is mostly horizontal: the puff vertical size reaches the top of the first vertical level (30 m) after only a few time steps. Besides, the Gaussian puff model allows to better represent the vertical diffusion, which the Eulerian model underestimates in the vicinity of the source. This mechanism is highlighted in this section, along with the sensitivity to the local-scale dispersion parameterizations.

4.1. Local-Scale Dispersion Parameters

[43] Figure 8 shows the evolution of σ_y and σ_z for the three parameterizations, for a puff emitted during daytime (16:00 UTC, Figures 8a and 8b) and nighttime (2200 UTC, Figures 8c and 8d), during 3 h ($\sigma_y \simeq \sigma_x$). The tendency is similar over the next 9 h. The Pasquill stability class was D (neutral) during most of the emission. Thus, there is little difference between the standard deviations during nighttime and daytime, when computed with the Briggs and Doury parameterizations. Similarity theory, which relies on a more accurate description of the boundary layer (boundary height, Monin-Obukhov length) rather than on stability classes, shows more variability. The Doury parameterization, which shows the highest standard deviations, was fitted on tracer experiments conducted on wider fields than the usual experiments used to derive the Briggs formulae and the similarity theory formulae. Thus, the Doury scheme is better

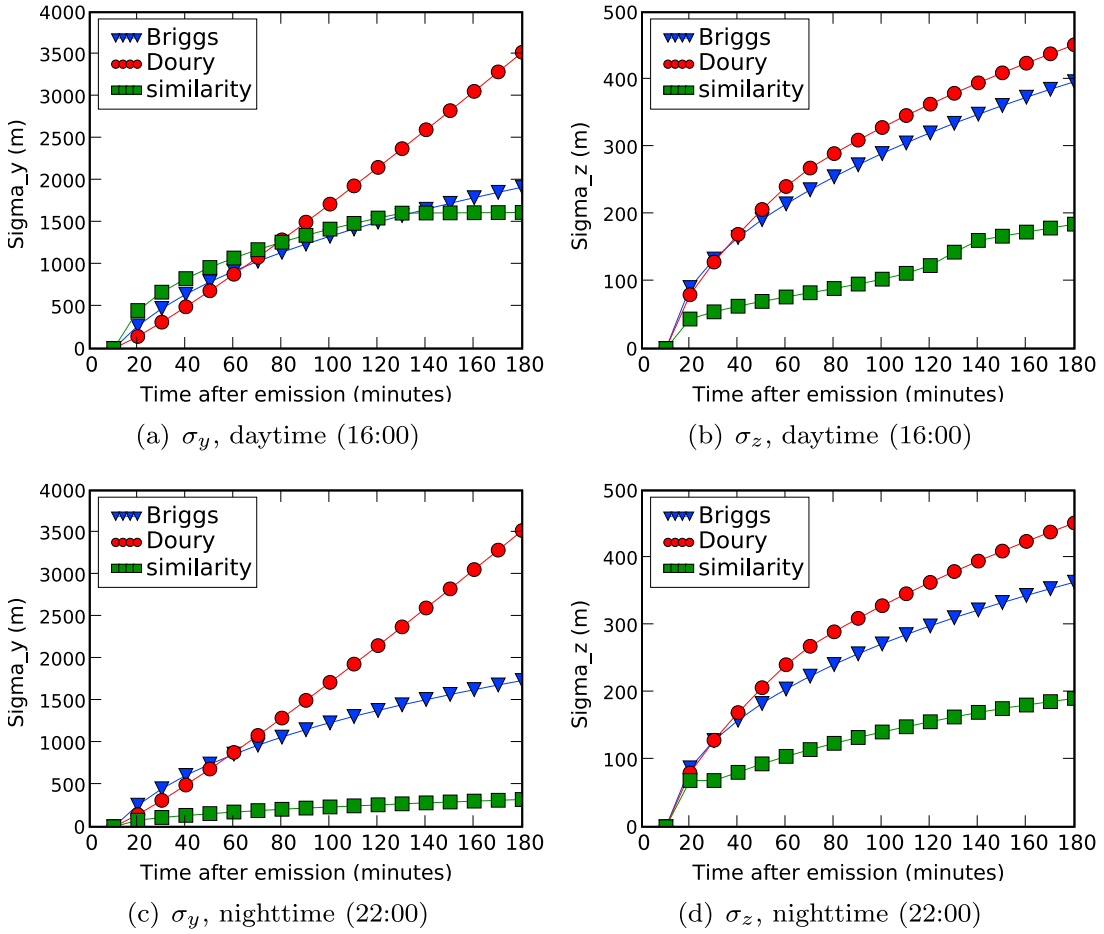

Figure 8. Evolution of the (a and c) horizontal standard deviation σ_y and (b and d) vertical standard deviation σ_z, during 3 h, for the three parameterizations and two puff release times. Figures 8a and 8b denote a puff emitted at the beginning of emission (1600 UTC). Figures 8c and 8d denote a puff emitted during the night (2200 UTC). The stability class is D (neutral).

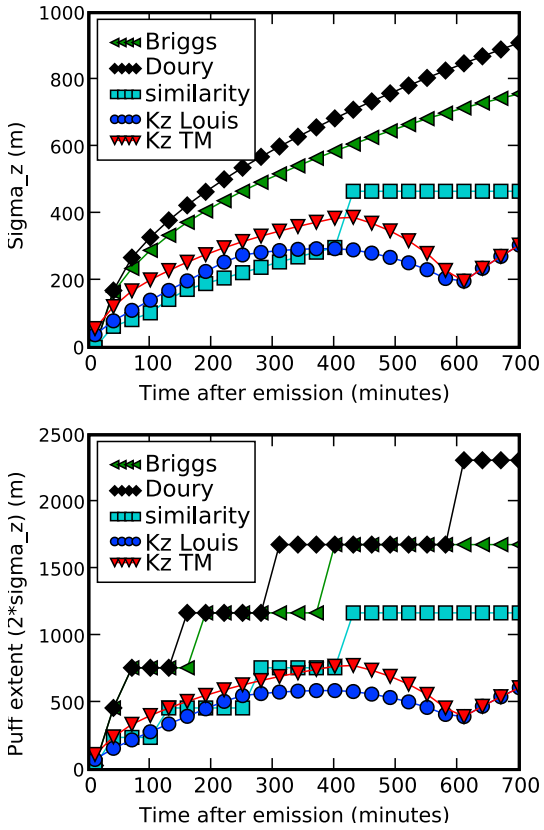

Figure 9. Evolution of the puff vertical extent during 12 h for the three Gaussian parameterizations, and for the two Eulerian parameterizations for K_z. (top) The puff extent is the Gaussian standard deviation σ_z. (bottom) The puff extent is the sum of the heights of the vertical levels covered by the puff. The puff extent is the same in both plots for the Eulerian parameterizations.

at European scale, while the other two parameterizations are better at local scale [*Korsakissok and Mallet*, 2009].

4.2. Comparison Between the Gaussian and Eulerian Diffusion

[44] The Eulerian model represents the turbulence through the vertical diffusion coefficient K_z, which is parameterized and depends on the meteorological conditions. On the other hand, the Gaussian equation derives from the same dispersion equation as the Eulerian model, but simplified, especially by assuming a constant and homogeneous wind. Under these assumptions, the standard deviation σ_z can be related to the vertical diffusion coefficient K_z [*Seinfeld and Pandis*, 1998],

$$\sigma_z = \sqrt{2K_z t}. \tag{9}$$

Thus, the plume evolution computed with the Eulerian model has a behavior in $\sigma_z \propto \sqrt{t}$, which represents well the plume dispersion at long range, but underestimates the dispersion at short range, where it is theoretically closer to a behavior in $\sigma_z \propto t$ [*Taylor*, 1921]. Gaussian models, fitted on short-range experiments, better represent this behavior by adapting the dispersion to the puff distance from source (or "age", t). This was shown for instance by *Demaël and Carissimo* [2008], where a CFD code and a Gaussian model are compared on short-range experiments. Figure 9 (top) shows the comparison between the evolution of σ_z given by the Gaussian models, and by equation (9), taking the value of K_z in the puff cell. Figure 9 (bottom) shows the puff vertical extent, that is given in practice by the sum of the heights of the vertical levels covered by the puff (see Figure 3). Figure 9 also shows K_z as computed by two possible parameterizations: *Louis*'s [1979] and *Troen and Mahrt*'s [1986]. The dispersions corresponding to the two parameterizations for K_z are lower than those estimated with Doury's and Briggs's formulae, but they are close to that of the similarity theory estimation without the additional dilution due to the injection.

[45] In this study, the Louis parameterization is used. Although the Troen-Mahrt parameterization ensures slightly more vertical diffusion (as seen on Figure 9), it did not give quite as good results. Thus, changing the Eulerian parameterization to ensure more diffusion does not allow to accurately represent point emissions near the source. The plume-in-grid model can be considered as a subgrid-scale diffusion scheme, which adapts to the puff distance from the source, and proves to be more efficient than the usual diffusion parameterizations. However, the model results are still sensitive to the Eulerian diffusion, as shown by *Brandt et al.* [1998] using the DREAM model. This study also highlighted the insufficient vertical diffusion given by Eulerian schemes, since an homogeneous mixing of the pollutants within the boundary layer was found to be more efficient than the two Eulerian parameterizations evaluated (the Louis and similarity theory schemes).

4.3. Vertical Profiles

[46] Coming back to the simulation results, the influence of the vertical diffusion schemes can be observed on Figure 10, which shows the vertical profiles of the mean concentration. The concentrations are averaged over the whole horizontal domain, and the vertical profile is plotted against the simulation time step. Figure 10a shows the profile for the reference simulation. The emission begins at time step 96, and the source emits during 12 h within the first vertical level. Hence, the concentration increases with time within this level during the emission period, and slowly diffuses on the vertical. Figures 10b–10d show the same vertical profiles for the plume-in-grid model in several configurations. There is indeed more vertical diffusion, especially during the emission time. This tendency is stronger with the column injection than with the integrated injection. The Doury parameterization also shows a higher vertical diffusion than similarity theory, which is consistent with the previous results (Figure 9).

5. Relevant Time Scales: A Study on the Injection Time

[47] The injection time determines how long the emission is handled by the Gaussian model. The sensitivity to this parameter therefore gives an insight on the relevant time scale for the use of the local-scale model, before the errors made in the Gaussian modeling approach, due to trajectory

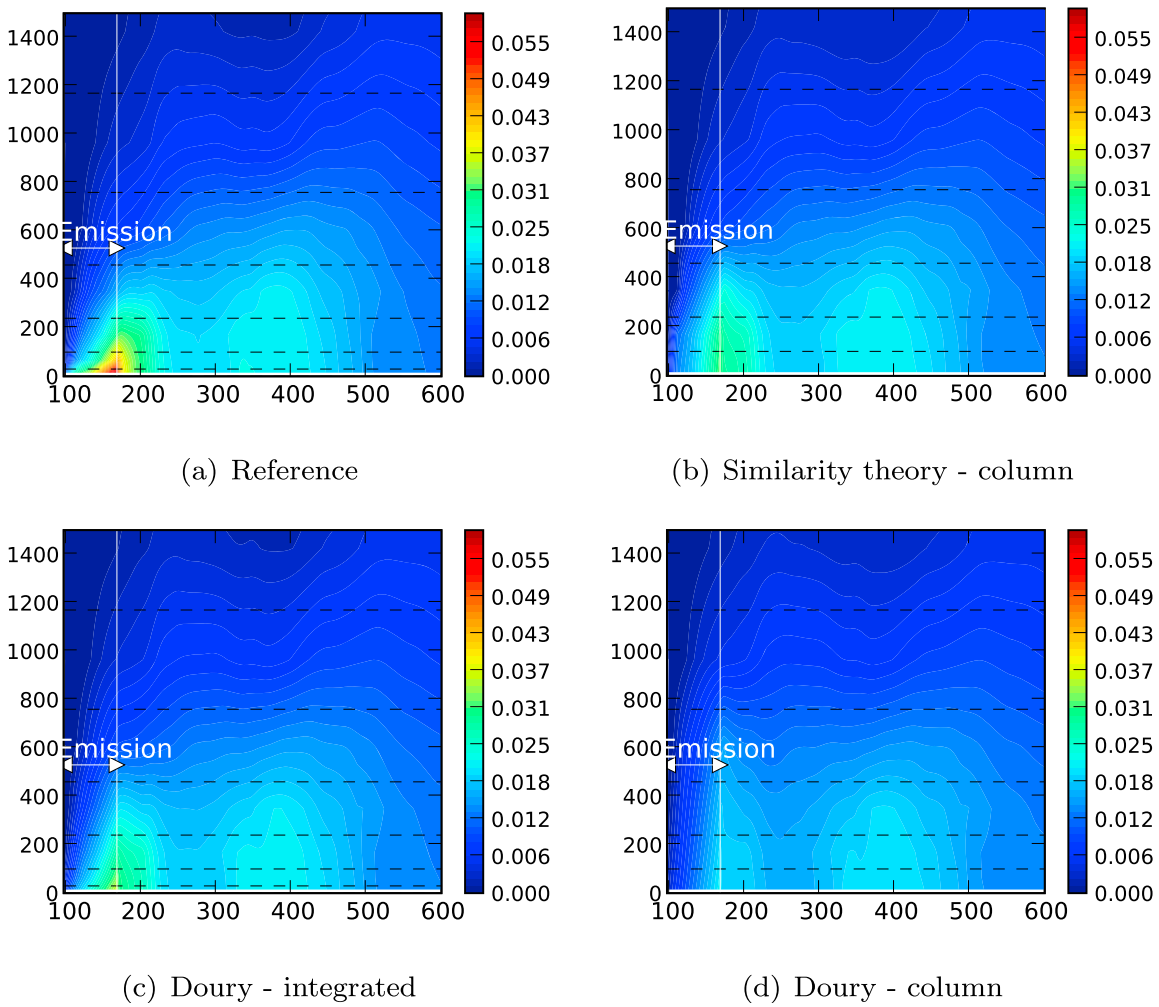

(a) Reference

(b) Similarity theory - column

(c) Doury - integrated

(d) Doury - column

Figure 10. Vertical profile of the concentrations (in μg m^{-3}), averaged over the whole horizontal domain. Ordinate gives vertical levels (meters); abscissa gives simulation time step (Δt = 600 s). The plume-in-grid injection time is 1 h. The horizontal lines represent the interfaces of the model vertical levels.

uncertainties as well as wind shear, become too large. For that purpose, plume-in-grid simulations were carried out with various injection times, ranging from t_{inj} = 0 to t_{inj} = 3 h with a discretization step of 10 min, and ranging from t_{inj} = 0 to t_{inj} = 12 h with a discretization step 1 h. The puffs are injected at the end of the time step (600 s) when the injection criterion is met.

5.1. Impact on the Concentrations

[48] Figure 11 shows the evolution of two statistical indicators presented section 3 (correlation and fractional bias) against the injection time. The trends are the same for the three parameterizations. Similarity theory does not give as good a bias as the two others but still much better than the reference simulation (dashed line). The Briggs parameterization gives a lower correlation than the reference simulation for almost all injection times. The correlation is more sensitive to the parameterization than other indicators (not reported here), especially between 0 and 3 h, while the bias is always good. As shown in section 3, the main impact of plume-in-grid on concentrations is localized in the vicinity of the source, which explains why even small injection times have an impact on the global results.

5.2. Impact on the Arrival Times

[49] Figure 12 shows the same indicators computed for the arrival times at the stations. The statistics are computed on values averaged over 3 h, and the arrival time is the first time period of 3 h when the mean value at the station is above the threshold value. This explains why the statistics are so good: the simulation has essentially to predict the plume arrival within 3 h of the observation to be considered as "perfect." These statistics are sensitive to the use of a plume-in-grid treatment: since the Eulerian model diffuses the plume more rapidly on the horizontal, it shortens the plume arrival time at stations. Using the plume-in-grid model delays this arrival, and the higher the injection time is, the later the plume arrives at the stations. Between 0 and 180 min, the correlation increases and the bias is almost constant. Between 3 and 12 h, however, the correlation and bias become worse than the reference simulation. Thus, an injection time of 3 h seems to be the upper limit for

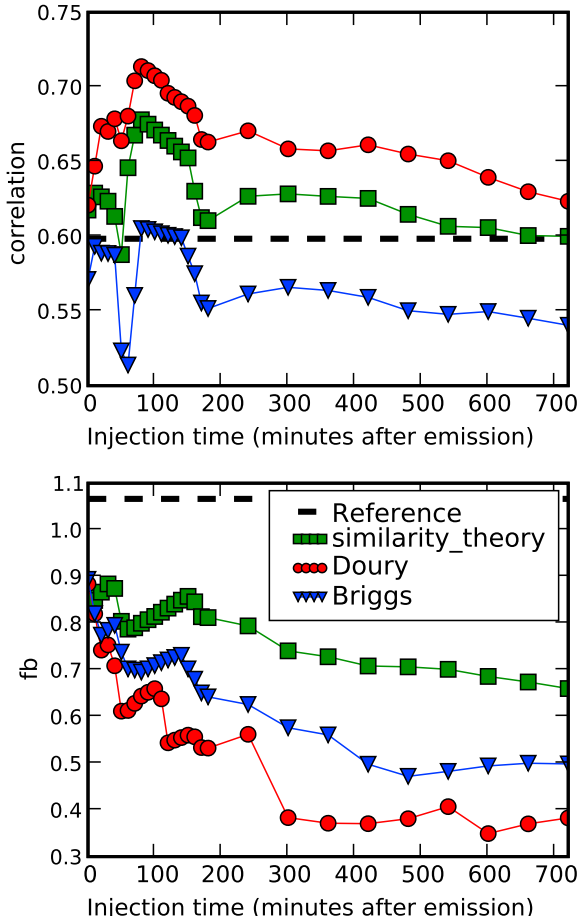

Figure 11. Evolution of the (top) correlation and (bottom) fractional bias against the puff injection time, ranging from 0 to 12 h. Statistics are computed for all concentrations and all stations. The simulations are carried out with the column injection for all three Gaussian parameterizations.

acceptable results, both for the arrival time and the concentrations statistics.

6. Influence of the Grid Resolution

[50] The spatial impact of the plume-in-grid treatment is now assessed from the viewpoint of the sensitivity to the grid resolution. The aim is to determine at what grid resolution the subgrid-scale treatment is more relevant, and to investigate the possible relationship between the grid resolution and the injection time. The grid resolution used in the previous parts of this study is henceforth called the "original" grid resolution; it corresponds to a cell size equal to 0.5625° (in longitude and latitude). Simulations were carried out for finer grids (÷8, ÷4, ÷2) and coarser grids (×2, ×4, ×6 and ×8). All the input data are the same as with the original resolution, except that they are interpolated (from the raw ECMWF data) at the new resolution. Hence, a finer resolution does not enhance the description of parameters such as the meteorological situation, and only the numerical impact of the grid resolution is assessed. This is consistent with our main goal, which is to improve the modeling of emissions without depending too much on the input data accuracy. Besides, the aim of such a model is to be used in an operational case, when no high-quality data are available, and the computational time is limited.

6.1. Impact of the Initial Volume of the Emission

[51] Before comparing the results with and without plume-in-grid, it is useful to assess the impact of the resolution on the Eulerian model alone. In particular, since the simulations are carried out with the same input parameters for all resolutions, the main changes may come from the initial volume of the emission: in the Eulerian model, the point source is immediately diluted within the volume of the cell where the source is located. Since the model has a tendency to overpredict the concentrations, a smaller emission volume will clearly increase this deficiency. To verify this hypothesis, the Eulerian model Polair3D was run on the finest grids (÷8, ÷4, ÷2), for two configurations. In the "reference" configuration, the source is emitted in one cell, as usual. The "diluted emission" consists in distributing the source in several cells, so that the total emission volume is equal to the cell volume of the original grid resolution. The result is shown in Figure 13. With the emission released in a single cell, the model statistics are worse with finer resolutions than with the original resolution. The FAC2 and FAC5 are less sensitive to emission changes, as already observed in section 3. On the contrary, the change in the

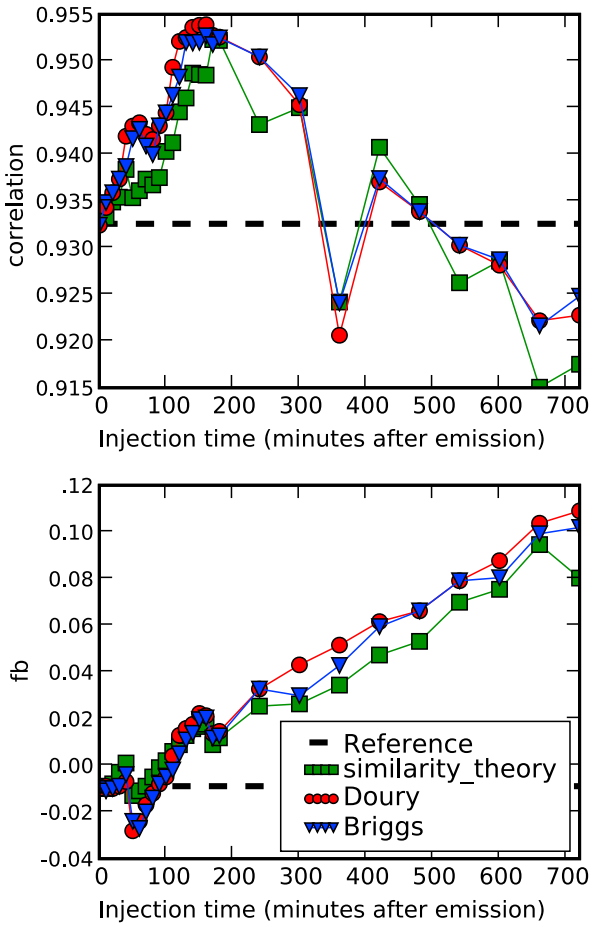

Figure 12. Evolution of the (top) correlation and (bottom) fractional bias for arrival times at stations, against the puff injection time. The simulations are carried out with the column injection for all three Gaussian parameterizations.

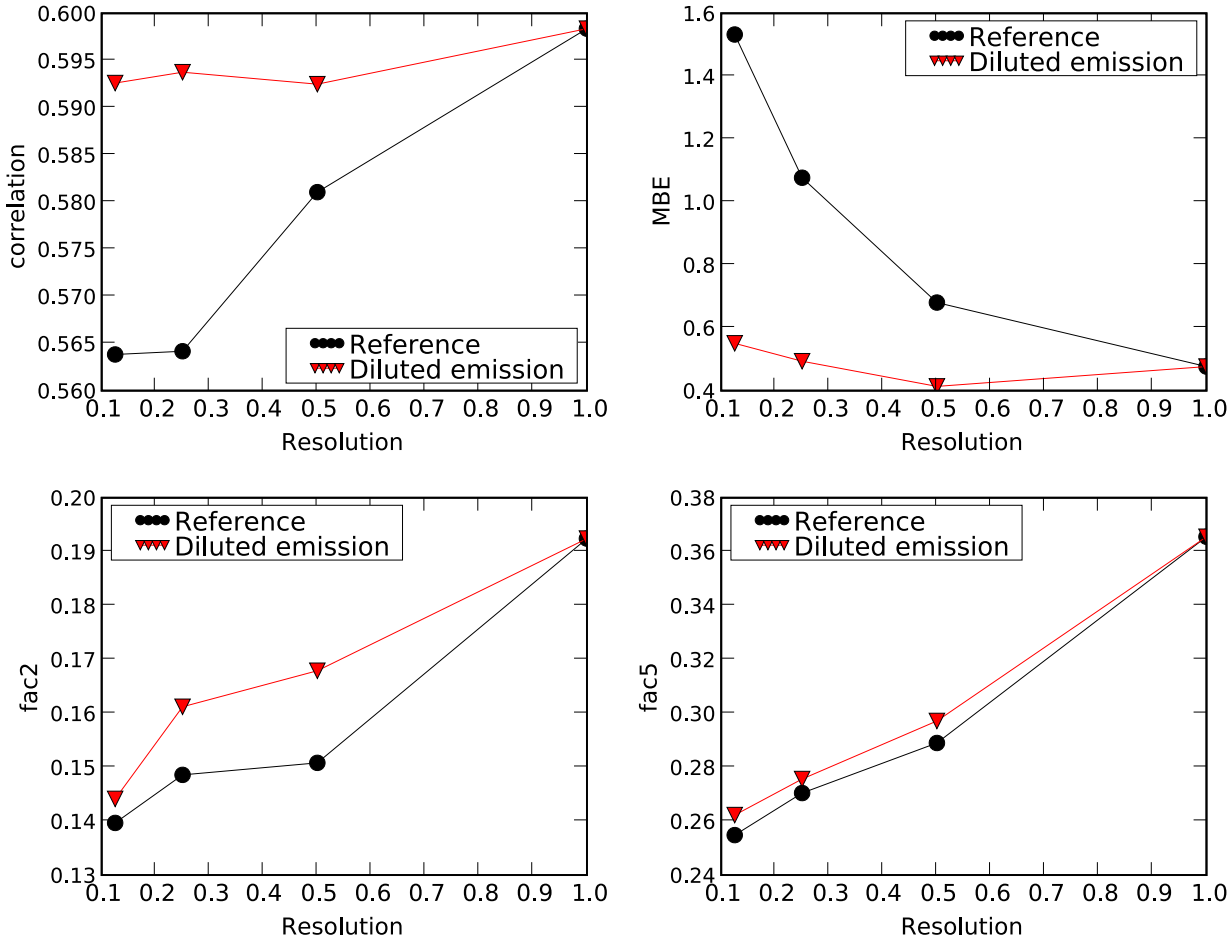

Figure 13. Evolution of the correlation, bias, FAC2, and FAC5 for the Eulerian model for several factors applied to the original grid resolution (÷8, ÷4, ÷2, and ×1). The label "Reference" is the simulation with the emission in one grid cell, and "diluted emission" refers to the simulations made with a constant emission volume.

emission volume is responsible for most of the decrease observed in the correlation and bias, when refining the resolution: with an unchanged emission volume, the correlation and bias are almost constant. This highlights the importance of the initial volume where the emission is released. In the Eulerian model, this volume depends on the grid resolution, and it would be difficult to find an "ideal" volume for any emission source, hence the need for a subgrid-scale treatment that limits the dependence.

6.2. Use of Plume-in-Grid With Several Grid Resolutions

[52] Figure 14 shows the impact of the grid resolution for Polair3D, as well as for the plume-in-grid model in several configurations. Several statistical indicators (correlation, mean bias error MBE, FAC2 and FAC5) are plotted against the grid resolution. In the sequel, the resolutions will be named after their abscissa in Figure 14: grid 0 is the finest (÷8), grid 3 is the original resolution, and grid 7 is the coarsest (×8). The reference simulation with Polair3D (dashed line) shows a decrease in performance for finer resolutions, as detailed in section 6.1. The best results of the reference simulation are given for grid 3 (original), grid 4 and grid 5.

[53] The plume-in-grid results are also shown for the three parameterizations and the two injection methods, with a 1 h injection time. The spread of the statistics for these six simulations is wider for the finer resolutions. The use of plume-in-grid tends to improve all the statistics for the fine resolutions (grid 0 to grid 3), in almost all cases. For coarser resolutions (grid 4 to grid 7), the results are globally close to the reference, or slightly worse (especially the correlations). The small spread in the output statistics for the coarse resolutions comes from the dilution of the puff concentrations within the cell, that smooths the differences between the parameterizations. The "best" injection time would depend on the grid resolution, as well as the parameterization, which makes it difficult to determine.

[54] The other injection criterion, based on the puff size, as defined in equation (7), is also evaluated. It has the advantage of adapting to the grid resolution. The results with the size injection criterion are shown in Figure 15, with $C_y = 8$; the puff is injected when it reaches half the cell size. They are quite good for fine resolutions: they are better, especially in terms of bias, than the 1 h results (Figure 14). However, the results with the original resolution (grid 3) and coarser resolutions are bad, especially for the correlation: the puffs are not injected before 6 h, or more, which

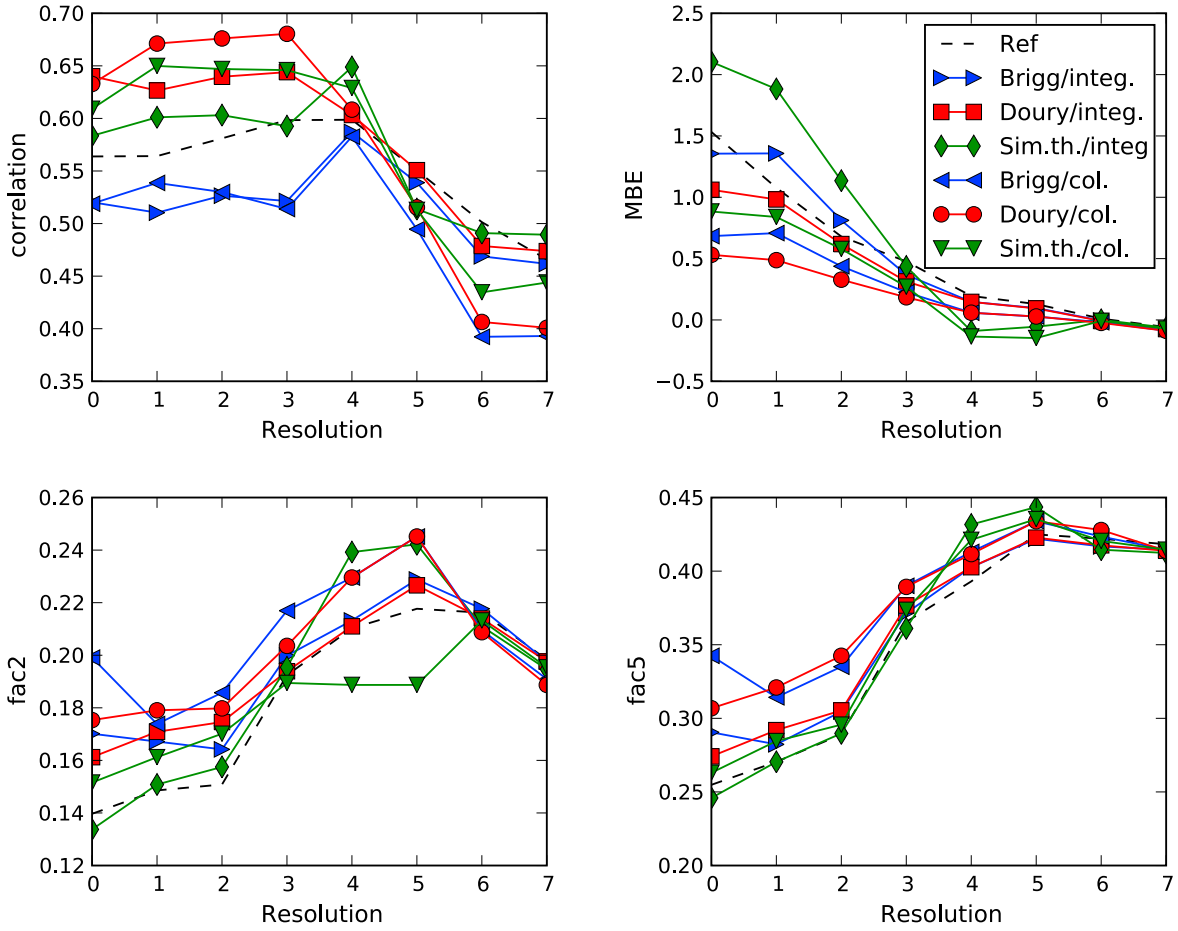

Figure 14. Evolution of the correlation, bias, FAC2, and FAC5 for reference and plume-in-grid models for several factors applied to the original grid resolution (÷8, ÷4, ÷2, ×1, ×2, ×4, ×6, and ×8). Statistics on concentrations for 139 stations. The injection time is 1 h.

leads to large errors in their trajectories. Thus, it is advised to use an injection criterion based on the puff size only for grid cells smaller than 25 km, and to ensure the puff injection time is no larger than 3 h.

7. Application to the Chernobyl Disaster

[55] An explosive accident took place at the Chernobyl nuclear power plant in Ukraine (51°23′N, 30°06′W), on 25 April 1986 at 2123 UTC. This disaster triggered a dispersion of radionuclides at continental scale. Radioactivity was measured in many European countries after the accident. The measured data used here come from the REM database (Joint Research Center, Ispra, Italy) and consist in 88 stations, scattered mainly through central and western European countries. While the ETEX case provided a well-documented case to carry out a comprehensive sensitivity study, Chernobyl is a means to evaluate the model in a real-case study with many uncertainties, especially concerning the source characteristics.

7.1. Modeling Setup

[56] The simulation was carried out with the ERA-40 fields from ECMWF, of 1.125° resolution. The simulation grid also has a 1.125° resolution in both horizontal directions. The simulation time step is 900 s and there are 12 levels, up to 5000 m. The plume-in-grid model is used with the column injection and the Doury parameterization, and a 3 h injection time (chosen because of the very coarse resolution).

7.1.1. Species

[57] The released radionuclides were both particulate matter and gaseous species. Here, we model only iodine (I^{131}) and caesium (Cs^{137} and Cs^{134}) in a gaseous form. For this model evaluation, we have chosen to use a simple modeling of the species dry deposition and scavenging coefficients, similarly to [*Quélo et al.*, 2007]. The deposition velocity is constant, equal to 0.2 cm s^{-1} for caesium and 0.5 cm s^{-1} for iodine. The scavenging coefficient is parameterized with the Belot formula [*Belot et al.*, 1988], as $\Lambda = Ap_0^B$, where p_0 is the rain intensity (in mm h^{-1}), $A = 8 \times 10^{-5}$ and $B = 0.8$. For a more comprehensive study of these parameterizations, we refer to *Brandt et al.* [2002]. The radioactive decay of the three species is taken into account, with half-life values of 8.04 days for I^{131}, 742 days for Cs^{134} and 11000 days for Cs^{137}.

7.1.2. Source Term

[58] The main uncertainties come from the estimation of the source. The total released activity and temporal distribution, as well as the vertical distribution, are highly

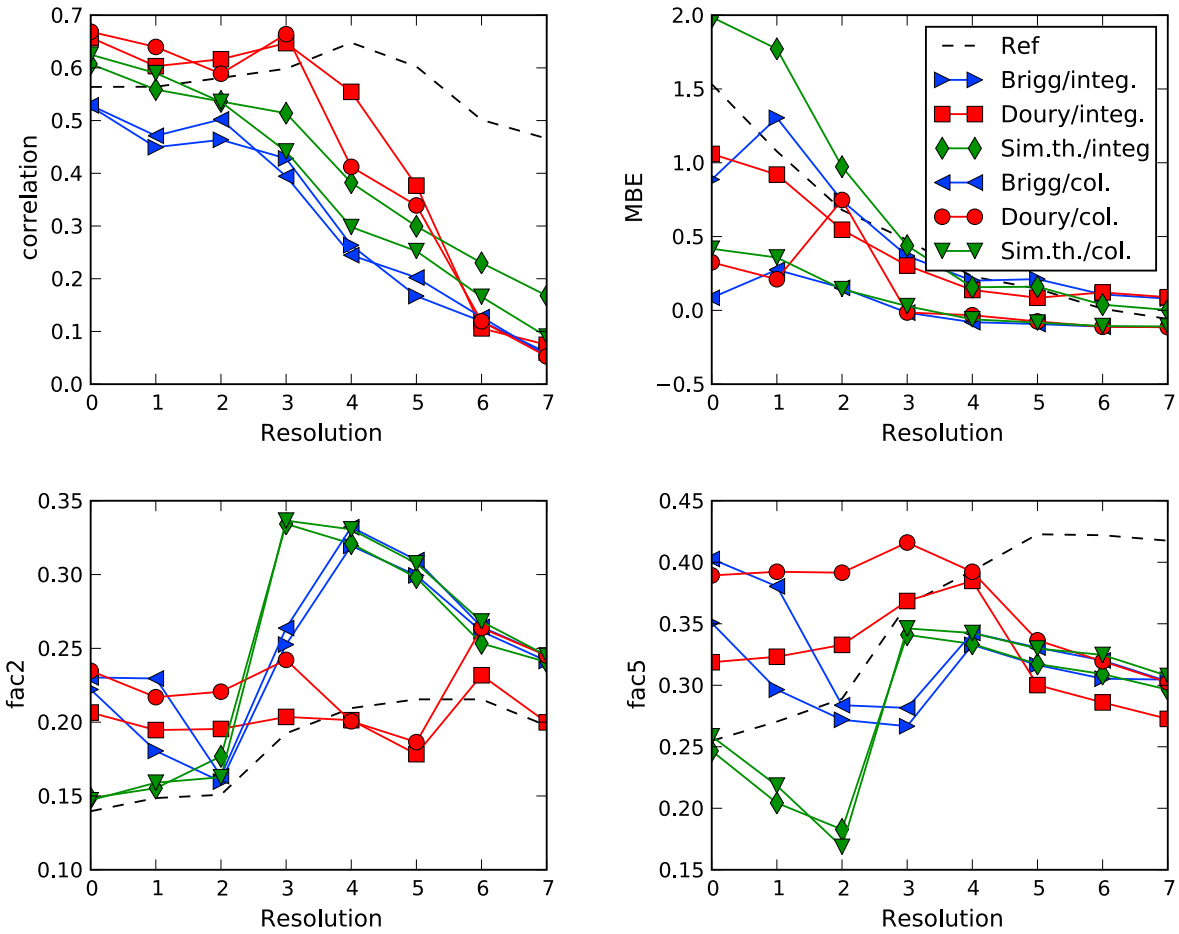

Figure 15. Evolution of the correlation, bias, FAC2, and FAC5 for reference and plume-in-grid models for several factors applied to the original grid resolution (÷8, ÷4, ÷2, ×1, ×2, ×4, ×6, and ×8). Statistics on concentrations for 139 stations. Plume-in-grid simulations use an injection criterion on the puff size.

uncertain: the high core temperature lead to very high effective release heights during the initial explosion, while the emission height was lower during the two following weeks. Here, we use the vertical distribution of *Brandt et al.* [2002]. Simulations are carried out with two estimations of the total activity and time evolution: one comes from *UNSCEAR* [2000] and was used by *Quélo et al.* [2007], while the other was constructed by inverse modeling, using Polair3D [*Davoine and Bocquet*, 2007]. The Polair3D configuration used for inverse modeling was the same as used here (same meteorological fields, simulation grid, species parameterizations). The temporal factors for the two sources are given in Table 3. The total estimated activity is: (1) I^{131}: 1.76×10^{18} Bq (UNSCEAR), 1.62×10^{18} Bq (reconstructed); (2) Cs^{137}: 8.5×10^{16} Bq (UNSCEAR), 13.6×10^{16} Bq (reconstructed); and (3) Cs^{134}: 5.4×10^{16} Bq (UNSCEAR), 3.5×10^{16} Bq (reconstructed).

7.2. Results

[59] In this case, there are no stations in the vicinity of the source: the smallest arrival time is 3 days after the explosion. Hence, even though using a plume-in-grid model still has an impact on the global statistics, the model results are quite insensitive to the local-scale configuration. Table 4 shows the models statistics with the UNSCEAR source term as well as the source term reconstructed by inverse modeling, for the three species. The source term specification is, as expected, the most important parameter, and has much more influence on the results than the model in use. The comparison with and without plume-in-grid with the

Table 3. Temporal Factors for the Chernobyl Emission for the UNSCEAR Source Term and the Source Term Coming From Inverse Modeling[a]

Factors	26 April	27 April	28 April	29 April	30 April	1 May	2 May	3 May	4 May	5 May
UNSCEAR	0.40	0.116	0.085	0.058	0.039	0.035	0.058	0.061	0.074	0.074
Inv. Mod.	0.45	0.42	0.05	0.001	0.015	0	0.015	0.01	0.01	0.032

[a]Factors are given for each day and applied to the total emission rate. Inv. Mod., inverse modeling.

Table 4. Chernobyl Statistics for the UNSCEAR Source Term and the Source Term Reconstructed With Inverse Modeling[a]

Model	Mean Observation	Mean Simulation	MBE	NMSE	Corr	FAC2	FMT
UNSCEAR							
Cs^{137}	0.98	0.49/0.48	−0.49/−0.50	5.62/5.73	0.46/0.47	0.23/0.26	0.31/0.31
Cs^{134}	0.57	0.34/0.33	−0.23/−0.23	4.77/4.88	0.46/0.47	0.26/0.28	0.33/0.33
I^{131}	3.83	3.45/3.42	−0.36/−0.40	6.08/6.37	0.43/0.39	0.34/0.35	0.36/0.35
Inverse modeling							
Cs^{137}	0.98	1.3/1.2	0.32/0.23	3.01/2.52	0.53/0.56	0.39/0.41	0.42/0.45
Cs^{134}	0.57	0.36/0.34	−0.20/−0.23	4.06/4.26	0.54/0.57	0.33/0.34	0.39/0.39
I^{131}	3.83	5.59/5.18	1.76/1.35	6.06/5.43	0.47/0.47	0.38/0.39	0.36/0.39

[a]Statistics are given in the following order: reference/plume-in-grid. The plume-in-grid simulations are run with a 3 h injection time, the Doury parameterization, and the column injection.

UNSCEAR source term does not show a significant trend. The plume-in-grid results tend to be better in terms of FAC2 but slightly more biased. Using the plume-in-grid model with the reconstructed source term shows, however, a clear tendency to improve all indicators, even when looking at the performance at stations (not shown). Since the inverse modeling was performed with Polair3D (without plume-in-grid), this configuration is optimized for the reference model, but the plume-in-grid model performs better nonetheless. However, these results confirm that the use of a plume-in-grid model is mostly efficient at "local-scale" stations, and that no significant improvement can be expected when stations are located so far from the source.

8. Conclusions

8.1. Physical Processes

[60] The plume-in-grid treatment of the point source emissions implemented within Polyphemus is described in this paper, with an emphasis on the available parameterizations for the local-scale dispersion and the model coupling. The associated study, based on the ETEX passive tracer experiment, shows that the main role of the plume-in-grid model is to better represent the vertical diffusion in the vicinity of the source. This theoretical result, and its practical implications, were analyzed. The subsequent improvement can be observed on the statistics on concentrations, especially at the closest stations to the source, and up to a few hundreds of kilometers from the release location. Thus, the scale of the plume-in-grid impact is much larger than the mere local-scale domain, where the Gaussian model is used. There is also an impact on the arrival times at all stations, that are more accurate with the delay implied by the plume-in-grid.

8.2. Sensitivity to the Local-Scale Parameterizations

[61] While the results with plume-in-grid are almost always better than with the Eulerian model alone, there is a substantial variability in the outputs when changing the parameterizations and injection method. The Doury parameterization is found to be the best in this case, ensuring more vertical diffusion. The column injection gives slightly better results than the integrated injection for the same reason. The sensitivity to the local-scale parameterizations is mostly seen at the few stations located in the vicinity of the source. As confirmed with the Chernobyl case, this sensitivity is much less important at farthest stations.

8.3. Spatial and Time Scales

[62] The upper time limit, for the use of the local-scale model, was found to be about 3 h. Afterward, the global statistics on the concentrations and the arrival times tend to worsen. This can be observed in the ETEX case and in the Chernobyl case as well (not shown here). The use of a plume-in-grid coupling tends to be more efficient at finer resolutions: it allows to depend less on the volume of the Eulerian cells, and to compensate for the subsequent overprediction. The key point when using the plume-in-grid model is to determine a good injection time. It is proposed here to use a criterion on the puff size when the resolution is finer than 25 km. For coarser resolutions, this methods leads to very high injection times, and errors in the puff trajectory tend to decrease the model's performance. Using a fixed injection time (the default 1 h value seems appropriate in most cases) is therefore recommended.

8.4. Perspectives

[63] The results of this application and sensitivity study on the ETEX case are representative of near-ground releases during neutral conditions. However, the conclusions may be different for elevated releases, for instance, buoyant emissions from power plants may be released at 200 m or more. In these cases, the plume is maintained aloft for a longer time with the plume-in-grid model, especially during nighttime and very stable situations [*Karamchandani et al.*, 2002]. Thus, a next step could be to extend the plume-in-grid model to reactive cases, to be evaluated with elevated releases. Another step could be to use the plume-in-grid model for inverse modeling and network design studies. Using higher resolution meteorological data, or a local meteorological model (diagnostic or pronostic) in the vicinity of the source could also bring significant improvements.

Appendix A: Coordinates

[64] Since Polair3D uses longitude and latitude coordinates, and the Gaussian model uses Cartesian coordinates, it is necessary to carry out a coordinate transformation. The Cartesian coordinates are the coordinates in the tangent plane at the point source. The transformation formulae are

$$\begin{pmatrix} \mathrm{d}x \\ \mathrm{d}y \end{pmatrix} = \begin{pmatrix} R\cos\phi\,\mathrm{d}\lambda \\ R\mathrm{d}\phi \end{pmatrix}, \tag{A1}$$

where x, y, z are the point Cartesian coordinates, λ is the longitude and ϕ is the latitude, in radians, and R is the Earth radius in meters.

[65] Note that we assume that the distance between the source and the puff center is not too great, otherwise the error in assimilating the puff trajectory to that in the tangent plane could not be neglected anymore.

Appendix B: Formulae to Compute the Puff Integral Over a Volume

[66] Let a puff α contain a given quantity of species A. The concentration of A in α is denoted c_A^α. The integral over space of a variable v is denoted with brackets $\langle v \rangle$.

[67] The total quantity of A in the puff is given by

$$Q_A^\alpha = \langle c_A^\alpha \rangle = \int_{-\infty}^{\infty}\int_{-\infty}^{\infty}\int_{-\infty}^{\infty} c_A^\alpha. \tag{B1}$$

[68] If we assume that the puff has a Gaussian shape, then the concentration can be written as

$$c_A^\alpha(x,y,z) = Q_A^\alpha \times G_\alpha^x(x) G_\alpha^y(y) G_\alpha^z(z), \tag{B2}$$

where $G_\alpha^x(x)$ is the Gaussian distribution in the x direction,

$$G_\alpha^x(x) = \frac{1}{\sqrt{2\pi}\sigma_x}\exp\left(-\frac{(x-x_\alpha)^2}{2\sigma_x^2}\right), \tag{B3}$$

with x_α the puff center coordinate and σ_x the puff standard deviation in the x direction.

[69] We want to compute the integral of the puff within a given volume, noted Q_A^{vol}. We note x_1 and x_2 the lower and upper boundaries in the x direction, and with a similar notation for the y and z directions, we have

$$Q_A^{vol} = \int_{x_1}^{x_2}\int_{y_1}^{y_2}\int_{z_1}^{z_2} c_A^\alpha(x,y,z)\mathrm{d}x\mathrm{d}y\mathrm{d}z. \tag{B4}$$

Combining this with equation (B2) leads to writing

$$Q_A^{vol} = Q_A^\alpha \times H_\alpha^x(x_1,x_2) H_\alpha^y(y_1,y_2) H_\alpha^z(z_1,z_2), \tag{B5}$$

with

$$\begin{aligned} H_\alpha^x(x_1,x_2) &= \int_{x_1}^{x_2} G_\alpha^x(x)\mathrm{d}x \\ &= \underbrace{\int_{-\infty}^{x_2} G_\alpha^x(x)\mathrm{d}x}_{F_\alpha^x(x_2)} - \underbrace{\int_{-\infty}^{x_1} G_\alpha^x(x)\mathrm{d}x}_{F_\alpha^x(x_1)}. \end{aligned} \tag{B6}$$

[70] To compute the integral over the volume Q_A^{vol}, we rely on the cumulative distribution function $F_\alpha^x(u)$ for a normal distribution (in the x direction),

$$F_\alpha^x(u) = \frac{1}{\sqrt{2\pi}\sigma_x}\int_{-\infty}^{u}\exp\left(-\frac{(x-x_\alpha)^2}{2\sigma_x^2}\right)\mathrm{d}x\,. \tag{B7}$$

[71] It can be expressed with the function erfc(u) defined as

$$\mathrm{erfc}(u) = \frac{2}{\sqrt{\pi}}\int_u^\infty \exp\left(-x^2\right)\mathrm{d}x, \tag{B8}$$

which satisfies erfc($-u$) = 1+ erf(u). A simple change of variable in equation (B7) shows that

$$F_\alpha^x(u) = \frac{1}{2}\left[1 + \mathrm{erf}\left(\frac{u-x_\alpha}{\sqrt{2}\sigma_x}\right)\right]. \tag{B9}$$

This allows to compute the integral over a given volume for a Gaussian-shaped puff. To take into account the reflections on the ground and capping inversion, additional reflection terms are needed, and their integral is computed following the same procedure.

[72] The cell concentration is corrected to ensure mass conservation: if Q_A^i is the mass of species A within the cell i (whose volume is V_i), then the puff contribution in this cell is given by

$$c_A^i = \frac{Q_A}{\sum_{i=1}^{N_{\mathrm{grid}}} Q_A^i} \times \frac{Q_A^i}{V_i}, \tag{B10}$$

where Q_A is the total mass of the puff for the species A, and N_{grid} is the number of cells into which the puff is transferred.

Appendix C: Statistical Indicators

[73] Here, C_p and C_0 are the sets of predicted and measured concentrations, respectively, $\overline{\alpha}$ is the average of value α over the data set (that is, for all times and stations), and σ_α is the standard deviation over the data set. Note that $\overline{C_0} - \overline{C_p}$ is used to define the bias, instead of $\overline{C_p} - \overline{C_0}$: this convention comes from the US EPA. This leads to negative values of FB and MBE for model overprediction and positive values if the model tends to underpredict concentrations.

$$\mathrm{MBE} = \overline{C_0} - \overline{C_p}, \tag{C1}$$

$$\mathrm{FB} = \frac{\left(\overline{C_0} - \overline{C_p}\right)}{0.5\left(\overline{C_0} + \overline{C_p}\right)}, \tag{C2}$$

$$\mathrm{NMSE} = \frac{\overline{\left(C_0 - C_p\right)^2}}{\overline{C_0}\,\overline{C_p}}, \tag{C3}$$

$$\mathrm{Corr} = \frac{\overline{\left(C_0 - \overline{C_0}\right)\left(C_p - \overline{C_p}\right)}}{\sigma_{C_0}\sigma_{C_p}}, \tag{C4}$$

$$\mathrm{FAC2} = \%\ \text{of data that satisfies}\ 0.5 \le \frac{C_p}{C_0} \le 2.0, \tag{C5}$$

$$\mathrm{FAC5} = \%\ \text{of data that satisfies}\ 0.2 \le \frac{C_p}{C_0} \le 5.0, \tag{C6}$$

$$FMT = \frac{\min\left(C_0, C_p\right)}{\max\left(C_0, C_p\right)}. \tag{C7}$$

The FMT stands for "figure of merit in time," and it measures the percentage of overlap of the measured and predicted areas above a threshold. It is actually called FMT when computed at a given location (for all times), FMS when computed for all stations at a given time, and simply FM for all stations and times. Here, it is always denoted FMT.

[74] **Acknowledgments.** We thank Christian Seigneur for his helpful advice and Bruno Sportisse for proposing this topic and offering suggestions along the work. We are also grateful to Marc Bocquet for providing data of the ETEX and Chernobyl cases and to Denis Quélo for his useful programs to compute the models' statistics.

References

Arya, S. (1999), *Air Pollution Meteorology and Dispersion*, Oxford Univ. Press, Oxford, U. K.

Belot, Y., C. Caput, and J. Guenot (1988), Etude bibliographique du lavage par la pluie des radionucléides particulaires et gazeux émis en situation accidentelle, technical report, Inst. de Radioprotection et de Sûreté Nucléaire, Fontenay-aux-Roses, France.

Bocquet, M. (2005), Reconstruction of an atmospheric tracer source using the principle of maximum entropy II: Applications, *Q. J. R. Meteorol. Soc.*, *131*(610), 2209–2223, doi:10.1256/qj.04.68.

Boutahar, J., S. Lacour, V. Mallet, D. Quélo, Y. Roustan, and B. Sportisse (2004), Development and validation of a fully modular platform for numerical modelling of air pollution: POLAIR, *Int. J. Environ. Pollut.*, *22*(1/2), 17–28.

Brandt, J. (1998), Modelling transport, dispersion and deposition of passive tracers from accidental releases, Ph.D. thesis, Natl. Environ. Res. Inst., Roskilde, Denmark.

Brandt, J., T. Mikkelsen, S. Thykier-Nielsen, and Z. Zlatev (1996), Using a combination of two models in tracer simulations, *Math. Comput. Modell.*, *23*(10), 99–115.

Brandt, J., A. Bastrup-Birk, J. Christensen, T. Mikkelsen, S. Thykier-Nielsen, and Z. Zlatev (1998), Testing the importance of accurate meteorological input fields and parameterizations in atmospheric transport modelling using DREAM—Validation against ETEX-I, *Atmos. Environ.*, *32*(24), 4167–4186.

Brandt, J., J. Christensen, and L. Frohn (2002), Modelling transport and deposition of caesium and iodine from the Chernobyl accident using the DREAM model, *Atmos. Chem. Phys.*, *2*, 397–417.

Byun, D., and K. L. Schere (2006), Review of the governing equations, computational algorithms, and other components of the models-3 Community Multiscale Air Quality (CMAQ) modeling system, *Appl. Mech. Rev.*, *59*(1–6), 51–77, doi:10.1115/1.2128636.

Davoine, X., and M. Bocquet (2007), Inverse modelling-based reconstruction of the Chernobyl source term available for long-range transport, *Atmos. Chem. Phys.*, *7*, 1549–1564.

Demaël, E., and B. Carissimo (2008), Comparative evaluation of an Eulerian CFD and Gaussian plume models based on Prairie Grass dispersion experiment, *J. Appl. Meteorol.*, *47*(3), 888–900.

Doury, A. (1976), Une méthode de calcul pratique et générale pour la prévision numérique des pollutions véhiculées par l'atmosphère, *Tech. Rep. 4280*, Commissariat à l'Énergie Atomique, Gif-sur-Yvette, France.

Hanna, S. (1984), Applications in air pollution modeling, in *Atmospheric Turbulence and Air Pollution Modeling*, edited by F. Niewstadt and H. van Dop, D. Reidel, New York.

Hanna, S., G. Briggs, and R. Hosker Jr. (1982), *Handbook on Atmospheric Diffusion*, Tech. Info. Cent., U. S. Dep. of Energy, Springfield, Va.

Irwin, J. (1979), Scheme for estimating dispersion parameters as a function of release height, *Tech. Rep. 600:4-79-062*, Environ. Prot. Agency, Washington, D. C.

Karamchandani, P., C. Seigneur, K. Vijayaraghavan, and S. Wu (2002), Development and application of a state-of-the-science plume-in-grid model, *J. Geophys. Res.*, *107*(D19), 4403, doi:10.1029/2002JD002123.

Korsakissok, I., and V. Mallet (2009), Comparative study of Gaussian dispersion formulae within the Polyphemus platform: Evaluation with Prairie Grass and Kincaid experiments, *J. Appl. Meteorol.*, *48*(12), 2459–2473, doi:10.1175/2009JAMC2160.1.

Kumar, N., and A. Russell (1996), Development of a computationally efficient, reactive subgrid-scale plume model and the impact in the northern United States using increasing levels of chemical details, *J. Geophys. Res.*, *101*, 16,737–16,744.

Louis, J.-F. (1979), A parametric model of vertical eddy fluxes in the atmosphere, *Boundary Layer Meteorol.*, *17*, 187–202.

Mallet, V., et al. (2007), Technical Note: The air quality modeling system Polyphemus, *Atmos. Chem. Phys.*, *7*, 5479–5487.

Maryon, R., and A. Buckland (1995), Tropospheric dispersion: The first ten days after a puff release, *Q. J. R. Meteorol. Soc.*, *121*(528), 1799–1833.

Morris, R., M. Yocke, T. Myers, and R. Kessler (1991), Development and testing of UAM-V: A nested-grid version of the urban airshed model, paper presented at Tropospheric Ozone and the Environment II, Air and Waste Manage. Assoc., Pittsburgh, Pa.

Mosca, S., G. Graziani, W. Klug, R. Bellasio, and R. Bianconi (1998), A statistical methodology for the evaluation of long-range dispersion models: An application to the ETEX exercise, *Atmos. Environ.*, *32*(24), 4307–4324.

Nodop, K., R. Connolly, and F. Girardi (1998), The field campaigns of the European Tracer Experiment (ETEX): Overview and results, *Atmos. Environ.*, *32*(24), 4095–4108.

Quélo, D., M. Krysta, M. Bocquet, O. Isnard, Y. Minier, and B. Sportisse (2007), Validation of the Polyphemus platform on the ETEX, Chernobyl and Algeciras cases, *Atmos. Environ.*, *41*(26), 5300–5315.

Ryall, D., and R. Maryon (1998), Validation of the UK Met. Office's NAME model against the ETEX dataset, *Atmos. Environ.*, *32*(24), 4265–4276.

Seigneur, C., T. Tesche, P. Roth, and M. Liu (1983), On the treatment of point source emissions in urban air quality modeling, *Atmos. Environ.*, *17*(9), 1655–1676.

Seinfeld, J. H., and S. N. Pandis (1998), *Atmospheric Chemistry and Physics: From Air Pollution to Climate Change*, Wiley-Intersci., Hoboken, N. J.

Sorensen, J. (1998), Sensitivity of the DERMA long-range Gaussian dispersion model to meteorological input and diffusion parameters, *Atmos. Environ.*, *32*(24), 4195–4206.

Stohl, A. (1998), Computation, accuracy and applications of trajectories—A review and bibliography, *Atmos. Environ.*, *32*(6), 947–966.

Stohl, A., and N. Koffi (1998), Evaluation of trajectories calculated from ECMWF data against constant volume balloon flights during ETEX, *Atmos. Environ.*, *32*(24), 4151–4156.

Taylor, G. (1921), Diffusion by continuous movements, *Proc. London Math. Soc.*, (20), 196–211.

Troen, I., and L. Mahrt (1986), A simple model of the atmospheric boundary layer: Sensitivity to surface evaporation, *Boundary Layer Meteorol.*, *37*, 129–148.

Turner, D. B. (1969), Workbook of atmospheric diffusion estimates, *Tech. Rep. 999-AP-26*, U.S. Environ. Prot. Agency, Washington, D. C.

UNSCEAR (2000), Annex J: Exposure and effects of the Chernobyl accident, technical report, U.N. Sci. Comm. on the Effects of At. Radiat., Vienna.

Weil, J. (1988), Dispersion in the convective boundary layer, in *Lectures on Air Pollution Modeling*, edited by A. Venkatram and J. Wyngaard, Am. Meteorol. Soc., Boston, Mass.

I. Korsakissok, CEREA, Université Paris Est, 6-8 av. Blaise Pascal, Cité Descartes, F-77455 Champs-sur-Marne, Marne la Vallée CEDEX 2, France. (korsakissok@cerea.enpc.fr)

V. Mallet, INRIA, Paris-Rocquencourt Research Center, B.P. 105, F-78153 Le Chesnay CEDEX, France. (Vivien.Mallet@inria.fr)